PAPER

NJC www.rsc.org/njc

# Preparation of multi-nanocrystalline transition metal oxide ($TiO_2$–$NiTiO_3$) mesoporous thin films

**David Ortiz de Zárate,[a] Cédric Boissière,[a] David Grosso,[a] Pierre-Antoine Albouy,[b] Heinz Amenitsch,[c] Pedro Amoros[d] and Clément Sanchez*[a]**

[a] *Laboratoire de Chimie de la Matière Condensée (CNRS), Université Pierre et Marie Curie, 4 place Jussieu, 75005 Paris, France. E-mail: clems@ccr.jussieu.fr; Fax: +33 (0)1 4427 4769; Tel: +33 (0)1 4427 3365*

[b] *Laboiratoire de Physique des Solides, Université Paris-Sud, 91405 Orsay, France*

[c] *Institute of Biophysics and X-ray Structure Research, Austrian Academy of Sciences, Steyrergasse 17/VI, 8010 Graz, Austria*

[d] *Instituto de Ciencia de Materiales, Universidad de Valencia, E-46071 Valencia, Spain*

***Received (in Montpellier, France) 19th October 2004, Accepted 19th November 2004***
***First published as an Advance Article on the web 14th December 2004***

Ordered mesoporous $TiO_2$–$NiTiO_3$ thin films, with nickel content $x < 0.5$, were prepared by dip-coating an acidic solution of hydrolysed transition metal chlorides in controlled humidity, followed by a very careful annealing treatment. These latter treatments were studied by *in situ* SAXS-WAXS experiments involving synchrotron radiation and TEM analysis. They revealed that the walls can be composed of amorphous, single crystalline or multi crystalline nanoparticles depending on $x$ and the conditions applied during the thermal treatment.



DOI: 10.1039/b416184j

## Introduction

Amongst the challenging tasks that need to be accomplished in the nanoscience domain by material scientists, the co-crystallisation of nanoparticles dispersed into a homogeneous matrix with an ordered mesostructure is crucial, as a result of the constant demands for novel and more integrated materials[1] as fundamental elements for electronic and spintronic devices, or as multifunctional matrices with a high accessibility for catalysis and chemical sensing. Such multicrystalline mesoporous ordered materials (MC-MOM) combine the physico-chemical properties of both crystalline phases (*e.g.*, conductivity, magnetisation, photo-activity, hardness, oxido-reduction, acid–base sites, chemical resistance,...) with the high surface-to-volume ratio associated with nano objects (*e.g.*, high surface of exchange between phases) and the high accessibility accompanying the ordered mesoporosity. Up to now, nanocrystalline transition metal oxide mesoporous materials were difficult to obtain by simple and direct sol-gel chemistry. One of the most successful approaches is reported in the literature as CMK materials (ordered Carbon Molecular Sieves). Their preparation usually implies the synthesis of 3D silica (or carbon) mesoporous powders.[2,3] This intermediate is then used as a high resistance template to stabilise and crystallise transition metal oxide amorphous sol-gel materials and the template is then dissolved or burnt (for silica or carbon matrixes, respectively). The CMK route, often decried as an expensive multi-step preparation, is an almost universal way for the preparation of very diverse nanocrystallised mesoporous powders. So far though, the CMK process has been inefficient for the preparation of mesostructured thin films, whose applications in industry are more attractive than powders due to much higher potential added value.

Nowadays, the only way to prepare such nanocrystalline mesoporous films is the EISA (evaporation induced self-assembly)[4] process, which allows in a single process the mesostructuration of numerous metal oxide structures. When followed by annealing at the proper temperature, ordered mesoporous transition metal oxides with nanocrystallised $TiO_2$, $ZrO_2$ or $Nb_2O_5$ walls were obtained as thin films[5–7] (or as powders[8]). Specific doping, such as $CeO_2$–$ZrO_2$ or $Y_2O_3$–$ZrO_2$,[9] was also possible and led to the desired stabilised crystallised phases. However, no mesoporous materials composed of well-dispersed and homogeneous nanoparticles with different metal oxide crystalline structures and chemical compositions have been reported so far, to the best of our knowledge.

The present work describes the preparation of mesoporous ordered thin films composed of amorphous Ni- and Ti-based oxides or nanocrystalline $TiO_2$ anatase, coexisting or not with $NiTiO_3$ ilmenite. Most of all, it demonstrates that the preparation of such a multi-crystalline network requires the total solubility of both cations in (i) the initial sol, (ii) the intermediate meso-organised hybrid phase, and (iii) the amorphous oxide phases before crystallisation. It will be shown that the latter and essential step of crystallisation requires a perfect control of the annealing conditions in order to achieve high crystallinity and a high degree of meso-ordering within a homogeneous association of mono-dispersed nanoparticles. The present statements are supported by *in situ*, time-resolved simultaneous SAXS and WAXS investigations during thermal treatment by using the 8 KeV SAXS beamline of the 3rd generation synchrotron ELETTRA (Italy) and TEM experiments.

## Results and discussion

Several films were prepared with various nickel contents, $x = [Ni]/([Ni] + [Ti])$, up to $x = 0.5$. It is likely that no inorganic-inorganic phase separation occurs during drying in the hybrid and amorphous porous states, since both the hexaaquo-$Ni^{2+}$ and $[Ti(OH)_2(H_2O)_{(4-x-y)}(Cl)_x(OEt)_y]^{(2-x-y)^+}$ species, stabilised in the present acidic conditions, are highly soluble in the (PEO, $H_2O$) hydrophilic phase and remain so even after

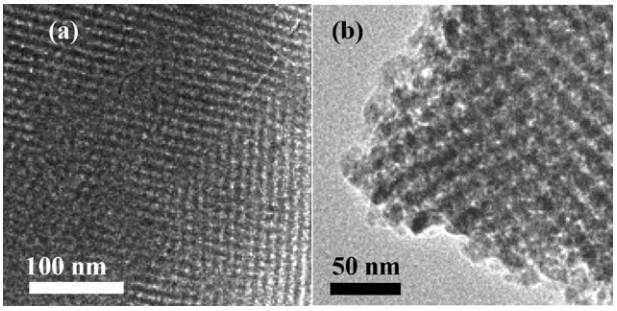


**Fig. 1** TEM image of (a) the $TiO_2$–$NiTiO_3$ ($x = 0.1$) structure after annealing at 300 °C shows an ordered mesostructure with discrete pores. The orientation observed is likely to correspond to a view along the [1–10] axis of an *Im*3*m* structure stretched along the [110] direction. In (b) is shown the mesostructure after annealing at 600 °C (where the 'grid-like' structure is evidenced).

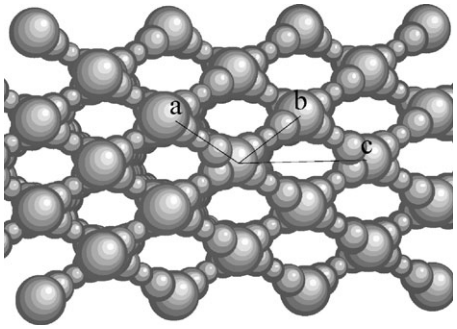


**Fig. 3** Scheme of the porous grid-like structure, resulting from the controlled diffusive sintering of the initial *Im*3*m* meso-ordered network,[11] taking place at high temperature after nucleation.



evaporation and departure of water.[5,10] We confirmed by XRD that neither crystalline nickel chloride nor nickel oxide exist within the films at studied temperatures. From TEM analysis (Fig. 1), films calcined at 300 °C exhibit a periodic porous structure coherent with an *Im*3*m* structure deformed along the [110] axis. This was confirmed by GI-SAXS measurements (Fig. 2). No evidence of phase separation out of the mesostructure was found for films annealed at any temperature. However, for temperature higher than 500 °C, HRTEM showed the existence of a nanoscale phase separation, which is discussed later. Between 510 and 680 °C, we confirmed that samples are entirely made of grid-like structure (shown schematically in Fig. 3) characteristic of the porous structure obtained after contraction along the [110] axis (a) and the diffused sintering (b) of the initial *Im*3*m* meso-ordered network prepared at low temperature. The complete transformation mechanism is described for pure $TiO_2$ in a previous paper.[11]

Periodicity between inorganic walls perpendicular to the surface was measured to be 9.9 nm, which corroborates the value deduced from the 2D-SAXS pattern of Fig. 2. These results are verified for $x \leq 0.3$, since the stoichiometric composition $x = 0.5$ leads to no order. *In situ*, time-resolved simultaneous SAXS and WAXS investigations during thermal treatment were performed for $x = 0.1$ and 0.3, as previously described.[11] Results are detailed in Fig. 2 for $x = 0.1$. 2D-SAXS patterns confirmed the TEM investigations since the diffraction spot indexation of the as-made film corresponds to a bcc *Im*3*m* symmetry contracted along the [110] direction [(110) planes are aligned with the surface]. The mesostructure unidirectional shrinkage orthogonal to the substrate is followed by transformation to a parallel grid-like porosity due to a crystallisation-induced diffused-sintering with increasing temperature (see Fig. 3). Eventually, the meso-order is lost upon extended sintering at temperatures higher than 680 °C.

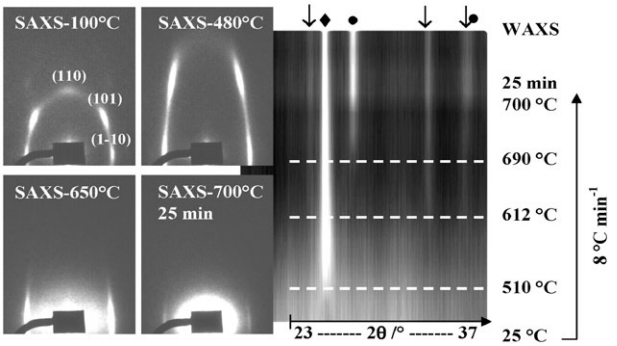


**Fig. 2** Simultaneous *in situ* 2D SAXS and 1D WAXS patterns recorded during the thermal treatment of a TiNi ($x = 0.1$) film. ◆, ●, and ↓ correspond to anatase (101); rutile (110) and (101); and ilmenite (012), (104) and (110) diffraction peaks, respectively, with increasing angles.

Despite the fact that the mesostructure of Ni–Ti films evolves in a similar trend as pure titania films, this is a different matter when regarding evolution of the wide angle diagrams with temperature for $x = 0.1$ Ni, given in Fig. 2. Nucleation of anatase [JCPDF 84-1286] usually takes place around 450 °C but is here retarded to 510 °C in the presence of 0.1 $Ni^{2+}$. In addition, the transformation into the more thermodynamically stable rutile phase [JCPDF 89-4920] occurs at 690 °C, while this latter transformation was not observed in the absence of $Ni^{2+}$ for temperatures up to 700 °C. This is somehow expected since $Ni^{2+}$ is known to catalyse the anatase-to-rutile transformation.[12] In-between these two critical temperatures of crystallisation for pure $TiO_2$, the bimetallic oxide $NiTiO_3$ [JCPDF 83-0212] ilmenite phase nucleation starts at 612 °C. As a result, since the mesostructure is completely lost after 3 min at 700 °C, $TiO_2$ anatase together with $NiTiO_3$ mesoporous ordered thin films can only be isolated by stopping the thermal treatment after reaching a temperature between 612 and 680 °C. The same limits were observed for $x = 0.3$, except that the anatase nucleation started at 550 °C. It is likely that the absence of the rutile transformation at high temperature for pure mesoporous $TiO_2$ films is related to the small size of the anatase crystallites, stabilised by the mesostructure.[11,13]

Films presenting coexisting anatase and ilmenite phases in a well-ordered mesoporous structure (optimally treated at 610–620 °C for $x = 0.1$ and 0.3) were further characterised by XRD in grazing incidence and HRTEM (see Fig. 4 and 5). Ellipsometry analyses showed that films were made of a single layer of homogeneous material, implying that the formation of Ti rich phases (anatase and rutile) and a Ni rich phase (ilmenite) did not lead to any layer phase separation but to a very localised phase separation within the walls. In such liquid deposition techniques, the molar ratio of $Ni^{2+}$ and $Ti^{4+}$ deposited on the substrate is expected to be that of the initial solution stoichiometry. Since only diffraction peaks associated to anatase and ilmenite are observed by XRD at

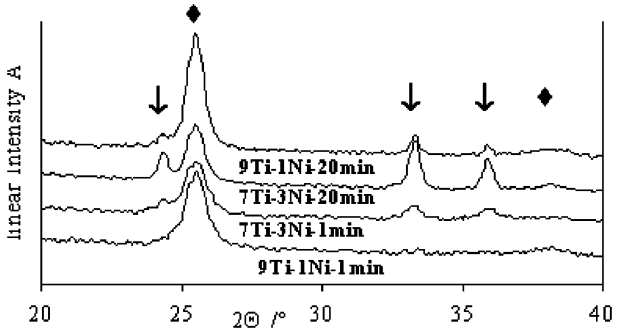


**Fig. 4** XRD diagrams of $TiO_2$–$NiTiO_3$ ($x = 0.1$ and 0.3) after annealing for 1 min or 20 min at 610 °C. ◆ and ↓ correspond to anatase (101) and ilmenite (012), (104) and (110) diffraction peaks, respectively, with increasing angles.

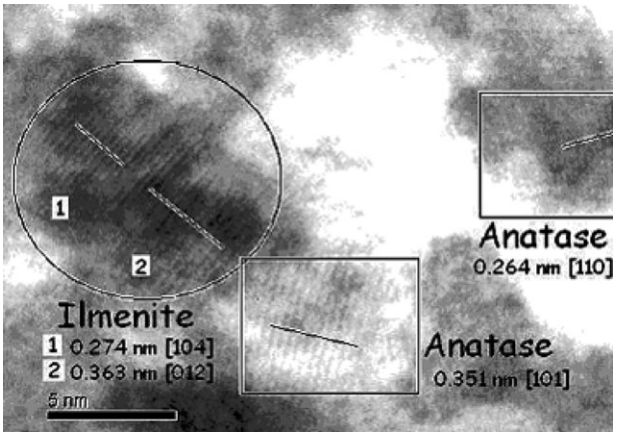


**Fig. 5** HRTEM image of mesoporous $TiO_2$–$NiTiO_3$ ($x = 0.1$) after annealing for 10 min at 620 °C, showing anatase and ilmenite nanocrystals coexisting at the edge of a mesopore.

this temperature, one assumes that 11% of $Ti^{4+}$ combines with the majority of $Ni^{2+}$, which leads to ≈10% molar of the $NiTiO_3$ phase.

These films exhibit an excellent optical quality (transparency > 99% in the wavelength range of 500 to 1000 nm) and a porosity of 40% in volume by ellipsometry. The Ni atomic concentration depth profile measured by RBS on around 100 nm thick films shows that Ni is well dispersed for $x = 0.1$ and 0.3, suggesting that the $NiTiO_3$ nanocrystals are homogeneously spread throughout the entire film bulk. The influence of the $Ni^{2+}$ content is deduced from Fig. 4, where diagrams of films containing either $x = 0.1$ or $x = 0.3$ $Ni^{2+}$ were recorded after annealing at 610 °C for 1 min or 20 min. Anatase and ilmenite particle dimensions, estimated by the Scherer formulae, are given in Table 1. When $x = 0.1$, the co-crystallisation takes place at $T_c = 610$ °C, as already observed by *in situ* WAXS, and more than 1 min at this $T_c$ is required to complete the nucleation process. The same observation can be done for $x = 0.3$, except that ilmenite peaks are more pronounced as a result of the higher initial stoichiometry in Ni (43% of $NiTiO_3$ when $x = 0.3$ *vs.* 11% when $x = 0.1$). As no NiO peaks were recorded (crystalline NiO forms usually between 400[14] and 500 °C), it is likely that most $Ni^{II}$ cations are incorporated into the ilmenite structure. The HRTEM image (see Fig. 5) of an annealed mesoporous $TiO_2$–$NiTiO_3$ film shows clearly the characteristic lattice plans of anatase and ilmenite phases, demonstrating that both nanocrystals coexist at the edge of the mesopores.

The nucleation steps are then followed by a diffuse sintering of the thinnest parts of the walls, leading to particle growth as detailed in Table 1. As seen on the SAXS patterns, the growth of anatase is responsible for the mesostructural rearrangement. The inorganic matter crystallisation mechanism seems then to take place as follows (see Fig. 6). First, the nucleation and growth of anatase at low temperature rejects the greatest portion of the nickel atoms to the edges of the anatase nanocrystals, creating a nanoscale phase separation with the appearance of a Ni-rich amorphous phase between anatase nanocrystals. A small part of the nickel atoms probably remains in the anatase crystalline structure, whose growth stops when the nickel and titania content become almost

**Table 1** Nanoparticle dimensions given in nm (±20%), deduced from the XRD peaks (Scherer's formulae)

| | Ti | 9Ti : 1Ni | 9Ti : 1Ni | 7Ti : 3Ni | 7Ti : 3Ni |
|---|---|---|---|---|---|
| Annealing time/min | 20[9] | 1 | 20 | 1 | 20 |
| $TiO_2$ | 12 | 9 | 12 | 8 | 10 |
| $NiTiO_3$ | — | — | 20 | 14 | 20 |

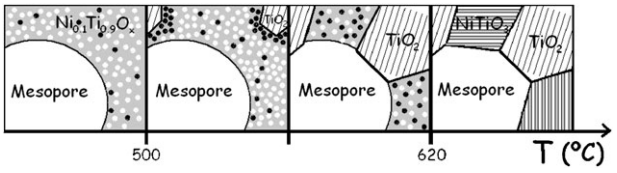


**Fig. 6** Cartoon of the crystallisation steps of $TiO_2$ and $NiTiO_3$ during thermal treatment.

similar in their vicinity, as predicted by the NiO–$TiO_2$ phase diagram.[15] Further increase in the temperature promotes the crystallisation of ilmenite from the amorphous nanodomains. This step does not seem to modify the meso-order of the MC-MOM. At higher $NiTiO_3$ concentration in the proximity of $TiO_2$, $TiO_2$ nucleates are spatially more separated. This effect could have been expected to prevent their easy diffusion/combination and hence their growth. Such a decrease in the anatase nanocrystal size with higher nickel content cannot be unambiguously observed by Scherer analysis (the size decrease is within the uncertainty of the measurement and, in any case, very close to pure anatase films). A possible explanation is that to be stable, anatase nanocrystals need to grow to a minimum size, which in this solid crystallisation process seems to be close to 10 nm. Finally, the minimum rutile crystal size phase being bigger than the anatase one, the rutile crystallisation promotes a massive rearrangement responsible for the mesostructure collapse.

## Conclusion

The synthesis of an ordered mesoporous material with anatase and ilmenite nanocrystals homogeneously distributed around the pores has been accomplished using sub-stoichiometric solutions of nickel and titanium. The extension to other systems could be potentially very interesting: different crystals (therefore different properties) around mesopores in a simple one-pot method of great versatility. In summary, the preparation of multi-crystalline mesoporous metal oxide thin films can be achieved by combining sol-gel chemistry, surfactant templating, liquid deposition techniques, and solid state chemistry. The present mesoporous $TiO_2$ containing $NiTiO_3$ material is the first example of many other possible combinations (perovskite, spinel, doping, *etc.*) that would open up a wealth of potential applications if these materials are associated with mesostructuration, high porosity, optical quality, high accessibility and high surface-to-volume ratio. The preparation of such materials will require perfect control of the conditions of the different steps involved, from the initial isotropic solution to the final multi-crystalline mesostructure.

## Experimental

Mixed $Ni^{II}$–$Ti^{IV}$ films were prepared by adapting the method reported for pure $TiO_2$ mesostructured films.[5] Typically, a very stable homogeneous sol was obtained by co-hydrolysing $TiCl_4$ and $NiCl_2$ in a mixture of ethanol and water in the presence of F127 ($EO_{70}PO_{106}EO_{70}$) block copolymer. The final molar ratio was $(1 - x)$ Ti : $x$ Ni : 40 EtOH : 10 $H_2O$ : 0.004 F127. Films were deposited by dip-coating on Si wafers [001] at a relative humidity (RH) of 40%. They were then allowed to dry overnight at RH = 60% before being annealed up to 700 °C at 8 °C $min^{-1}$ in air.

The *in situ* SAXS-WAXS experiment was performed at the SAXS beamline of the 3rd generation synchrotron ELETTRA (Italy), delivering the high flux of 8 KeV necessary for such an experiment. Films were disposed in the centre of a specially designed furnace heating at the rate of 8 °C $min^{-1}$ and equipped with apertures designed to allow the incident, the diffused and the diffracted radiation into and out of the heating

device without hindrance. The incident angle was fixed at $5^\circ \pm 1^\circ$ with the film surface in order to eliminate the specular reflection and the Yoneda signal from the detectors. The 2D-CCD camera was placed as to collect the global SAXS pattern every 2 min (10 s acquisition), while the linear detector was located such as to record diffraction taking place between $20^\circ$ and $40^\circ$ ($2\theta - \mathrm{CuK}\alpha$) and collect one diagram every 2 min (120 s acquisition) during the temperature rise. The meso- and microstructures were then deduced from the 2D and 1D diffraction patterns, respectively. The same films were additionally characterised by transmission electron microscopy (TEM) and high resolution transmission electron microscopy (HRTEM; JEOL 100 CX II), Rutherford back scattering (RBS) from which the number of atom per film volume unit and film porosity can be assessed with 10% error. VASE-Ellipsometry (Woollam M2000U) investigations provided the optical constants of the films.

## Acknowledgements

The authors thank Dominique Jalabert for his help with HRTEM. Also, David Ortiz de Zárate thanks the support of Spanish MCyT grant MAT 2000-1387-C02.

## References

1 (*a*) C. D. E. Lakeman and D. A. Payne, *Mater. Chem. Phys.*, 1994, **38**, 305; (*b*) S. A. Chambers and Y. K. Yoo, *MRS Bull.*, 2003, **28**, 706.
2 F. Gao, Q. Y. Lu and D. Y. Zhao, *Adv. Mater.*, 2003, **15**, 739.
3 B. Z. Tian, X. Liu, L. A. Solovyov, Z. Liu, H. Yang, Z. Zhang, S. Xie, F. Zhang, B. Tu, C. Yu, O. Terasaki and D. Zhao, *J. Am. Chem. Soc.*, 2004, **126**, 865.
4 (*a*) C. J. Brinker, Y. Lu, A. Sellinger and H. Fan, *Adv. Mater.*, 1999, **11**, 579; (*b*) D. Grosso, F. Cagnol, G. A. A. Soler Illia, E. L. Crepaldi, H. Amenitsch, P. A. Albouy, A. Brunet Brunneau, A. Bourgeois and C. Sanchez, *Adv. Funct. Mater.*, 2004, **14**, 309.
5 (*a*) D. Grosso, G. A. A. Soler Illia, F. Babonneau, C. Sanchez, P. A. Albouy, A. Brunet-Bruneau and R. Balkenende, *Adv. Mater.*, 2001, **13**, 1085; (*b*) E. Crepaldi, G. A. A. Soler Illia, D. Grosso, F. Cagnol, F. Ribot and C. Sanchez, *J. Am. Chem. Soc.*, 2003, **125**, 9770.
6 E. Crepaldi, G. A. A. Soler Illia, D. Grosso, P. A. Albouy and C. Sanchez, *Chem. Commun.*, 2001, 1582.
7 B. Lee, T. Yamashita, D. Lu, J. N. Kondo and K. Domen, *Chem. Mater.*, 2002, **14**, 867.
8 D. Grosso, G. J. A. A. Soler-Illia, E. Crepaldi and C. Sanchez, *Adv. Funct. Mater.*, 2003, **13**, 37.
9 E. L. Crepaldi, G. J. de A. A. Soler-Illia, A. Bouchara, D. Grosso, D. Durand and C. Sanchez, *Angew. Chem. Int. Ed.*, 2003, **42**, 347.
10 C. F. Baes and R. E. Mesmer, *The Hydrolysis of Cations*, Wiley-Interscience Publications, New York, 1976, p. 243.
11 D. Grosso, G. J. de A. A. Soler-Illia, E. L. Crepaldi, F. Cagnol, C. Sinturel, A. Bourgeois, A. Brunet-Bruneau, H. Amenitsch, P. A. Albouy and C. Sanchez, *Chem. Mater.*, 2003, **15**, 4562.
12 Y. H. Zhang and A. Reller, *Mater. Sci. Eng.*, 2002, **19**, 323.
13 M. Koelsch, S. Cassaignon, J. F. Guillemoles and J. P. Jolivet, *Thin Solid Films*, 2002, **403**, 312.
14 Z.-H. Liang, Y.-J. Zhu and X.-L. Hu, *J. Phys. Chem. B*, 2004, **108**, 3488.
15 *Phase Diagrams for Ceramists*, eds. R. S. Roth, J. R. Dennis and H. F. McMurdie, The American Ceramic Society, Inc., Columbus, Ohio, 1987, vol. **VI**, p. 129.